

Contents lists available at SciVerse ScienceDirect

Expert Systems with Applications

journal homepage: www.elsevier.com/locate/eswa



A new approach based on computer vision and non-linear Kalman filtering to monitor the nebulization quality of oil flames

A.T. Fleury a, F.C. Trigo b,*, F.P.R. Martins b

ARTICLE INFO

Keywords: Estimation of nebulization quality Non-linear Kalman filter Fuzzy logics Computer vision

ABSTRACT

The nebulization quality of oil flames, an important characteristic exhibited by combustion processes of petroleum refinery furnaces, is mostly affected by variations on the values of the vapor flow rate (VFR). Expressive visual changes in the flame patterns and decay of the combustion efficiency are observed when the process is tuned by diminishing the VFR. Such behavior is supported by experimental evidence showing that too low values of VFR and solid particulate material rate increase are strongly correlated. Given the economical importance of keeping this parameter under control, a laboratorial vertical furnace was devised with the purpose of carrying out experiments to prototype a computer vision system capable of estimating VFR values through the examination of test characteristic vectors based on geometric properties of the grey level histogram of instantaneous flame images. Firstly, a training set composed of feature vectors from all the images collected during experiments with a priori known VFR values are properly organized and an algorithm is applied to this data in order to generate a fuzzy measurement vector whose components represent membership degrees to the 'high nebulization quality' fuzzy set. Fuzzy classification vectors from images with unknown a priori VFR values are, then, assumed to be state-vectors in a random-walk model, and a non-linear Tikhonov regularized Kalman filter is applied to estimate the state and the corresponding nebulization quality. The successful validation of the output data, even based on small training data sets, indicates that the proposed approach could be applied to synthesize a real-time algorithm for evaluating the nebulization quality of combustion processes in petroleum refinery furnaces that use oil flames as the heating source.

© 2013 Elsevier Ltd. All rights reserved.

1. Introduction

Automatic diagnosis of technical defects in industrial plants has been a long date desire of the maintenance engineering community. Such an aim, however, can not be achieved unless the knowledge to detect an anomalous behaviour and to infer its most likely causes be properly represented and coded in order to emulate the ability of the expert responsible for the maintenance task. Various architectures of expert systems to deal with that class of problems have been proposed so far, encompassing rule-based (Qian, Li, Jiang, & Wen, 2003), Bayesian networks (Heo, Changa, Choib, Choic, & Jee, 2005), fuzzy rule-based (Azadeh, Ebrahimipour, & Bavar, 2010), neural networks (Calisto, Martins, & Afgan, 2008) and neural-fuzzy networks (Sahu, Padhee, & Mahapatra, 2011).

Automatically identifying faults in petroleum plants, however, imposes to the expert system developer some very strict demands. The project of a control system capable of optimizing the energetic efficiency of petroleum refinery furnaces in order to reduce the

emission rates of pollutants such as CO, NO_x and particulate material, requires the setting up of a large network of heterogeneous sensors (thermocouples, flow meters, air–fuel ratio gauges, opacity meters, pressure sensors etc.) dedicated to measure the main variables of the process and to give feedback to the controller. In the last two decades, however, video *CCD* (*Charged Coupled Device*) cameras and frame grabbers have been incorporated to this measurement apparatus, since image sequences of flames captured by a near infra-red sensitive *CCD* and properly analyzed by suitable computer vision methods may provide a large quantity of useful information to the controller.

Correlations between the brightness, spectral and geometric properties of flame images and the corresponding variables of the combustion process have been reported by several authors, who developed different methods to build characteristic vectors and use them to estimate a subset of the state variables that characterize a combustion point of operation. Among those methods, it is worthwhile citing neural networks (Santos-Victor, Costeira, Tomé, & Sencieiro, 1993), fuzzy rules based on triangular membership functions (Tuntrakoon & Kuntanapreda, 2003), hot spots identification through the application of thresholding and logical

a Centro Universitário da FEI, Av. Humberto de Alencar Castelo Branco, 3972, 09850-901 São Bernardo do Campo, SP, Brazil

^b Escola Politécnica da Universidade de São Paulo, Av. Prof. Mello Moraes 2231, 05508-930 São Paulo, SP, Brazil

^{*} Corresponding author. Tel.: +55 11 30915334; fax: +55 11 30915687. E-mail address: flavio.trigo@poli.usp.br (F.C. Trigo).

operators to a collection of sequentially grabbed images of flames (Bertucco, Fichera, Nunnari, & Pagano, 2000), spectral analysis of the hottest zones of flames obtained from images selected through a segmentation process (Baldini, Campadelli, & Lanzarotti, 2000), investigation of correlations between flame image measured parameters (area and centroid of the luminous region, ignition point position and spread angle) and physical data (particle size of the pulverized coals tested and mass flow rate of the primary air) and used them to build a characteristic vector of the combustion process (Yan, Lu, & Colechin, 2002; Yan, Lu, & Colechin, 2004, and Lu, Gilabert, & Yan, 2005), and self-organizing feature maps associated to cepstral analysis (Hernández & Ballester, 2008).

Particularly, a combustion diagnosis system developed by Wójcik and Kotyra (2009), based on the analysis of image flames captured at a frequency of 25 frames/s by an ordinary monochromatic video camera equipped with a fiberscope, uses a computer vision algorithm that generates, for each image of the temporal series, a characteristic vector whose components are shape parameters of the image flames, like area, perimeter, centroid coordinates and Fourier descriptors of their contours. Analyzing the temporal values of the shape parameters associated to oil flames exhibiting previously air-fuel ratios and different instability characteristics, the authors stress that there is a clear correlation among the parameters calculated and the phenomena examined, but do not present a method to automatically discriminate the flames according to the physical properties concerning the focused events. Similarly, using a set of four spatial luminous parameters (mean value, standard deviation, kurtosis and skewness of the spatio-temporal brightness image distribution) and one temporal spectral parameter (flicker frequency) extracted from flame images grabbed by a high-speed CCD video camera, the researchers in (González-Cencerrado, Peña, & Gil, 2012) investigated the relative influence of the above-mentioned parameters on combustion processes with different a priori known air-to-fuel ratios and combustion camera mean temperatures. Aided by multivariate regression methods, important correlations between the temporal evolution of both the image features and the respective combustion process variables could be identified: however, as admitted by the authors. an image feature based method to automatically characterize the combustion process should require a more thorough investigation.

In a research project developed at São Paulo State Institute of Technology (IPT) (Fleury, 2006), the authors of the present article proposed various computer vision algorithms to extract features of instantaneous and average flame images, in order to generate crisp decision rules that could be used to diagnose several kinds of abnormalities of the combustion process, encompassing: flame extinction, lack of symmetry, instability, high or low excess air and low nebulization quality. Despite the good agreement between the decisions issued by the application of those rules to image test sets and the known a priori physical conditions concerning the capture of such images, three drawbacks of this diagnostic system must be pointed out: firstly, it required the calculation of average images and the application of heterogeneous computer vision methods to generate the parameters used by the majority of the diagnostic decision rules, what imposed a limitation to the computational performance; secondly, only two states - either strict normality or abnormality of the process - could be diagnosed, although the decisions that can be made by a human expert on the combustion process are not so strict; finally, history of measurements were completely ignored, for the diagnostics were proposed on the basis of present measured values only.

In a further work (Fleury, Trigo, & Martins, 2010), the same authors focused the particular problem of identifying flames exhibiting nebulization patterns of low quality. As the experimental evidence indicate, such flames emerge from combustion mixtures with low values of *vapor flow rate* (i.e., the quotient between the

nebulization vapor flow and the fuel oil flow). After capturing images of flames from combustion processes with varied levels of VFRs, a dedicated diagnostic system was developed to classify them according to the nebulization patterns observed. Compared with the results reported in Fleury (2006), the performance of this new diagnostic system was much improved, due to the following changes: (i) feature vectors are based only on few properties of instantaneous images, which permit to apply simpler computer vision algorithms; (ii) fuzzy linguistic variables are used in the classification process, making the diagnostics more realistic; (iii) predictions are obtained through a stochastic minimum variance least squares estimator, giving rise to more reliable classifications.

The present research intends to validate the nebulization quality classification method described in Fleury et al. (2010) by applying it to sequences of images of flames whose values of *VFRs* are not known *a priori*, thus asserting the approach as an effective tool for combustion diagnostic. A Tikhonov-regularized version of the Kalman filter is used to estimate the state, a vector of properties from grabbed images. It must be emphasized that Sections 2 and 3 of this paper, which describe the currently used experimental setup and the procedure for obtaining the image feature vectors, contain extended versions of the material previously presented by Fleury et al. (2010).

2. Experimental apparatus and data collection

As illustrated in Fig. 1, the furnace used in the experiments at IPT is a vertical one, with the burner settled at the bottom and the gases exhaustion at the top. Having a total height of 4.0 m, it is subdivided in 12 independent water cooled blocks and can process number 1 fuel oil (number 1 fuel oils are distilled oils, i.e., they have low viscosity and are free of sediments and inorganic ash) at a maximum flow rate of 80 kg/h. The burner has two (primary and secondary) air entrances for natural air suction with manual flow regulation valves (Fig. 2).

In order to produce flame images of combustion processes exhibiting previously defined characteristics, it was necessary to monitor several significant variables, for which a data acquisition system connected to a heterogeneous network of measurement instruments had to be set up. Concerning the fuel, pressure was measured by a membrane-type manometer, mass flow by an oval gear meter equipped with a pulse generator, temperature by a type-T thermocouple. Monitoring of nebulization vapor variables required a membrane-type manometer, an orifice plate connected to a differential pressure sensor through seal pots and a type-T thermocouple, respectively for pressure, flow and temperature measurements. Regarding the emitted gases, a type-K

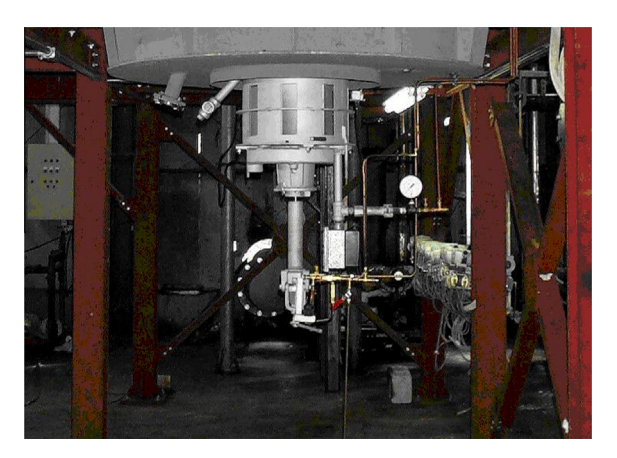


Fig. 1. Partial view of the vertical furnace used in the experiments.

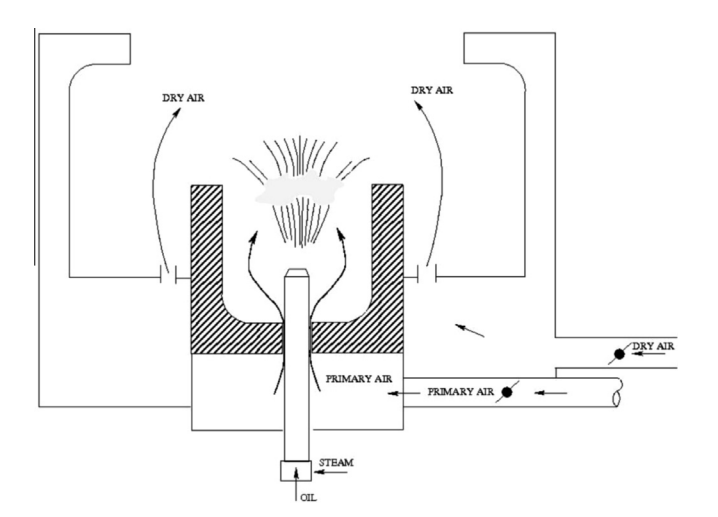


Fig. 2. Burner schematics.

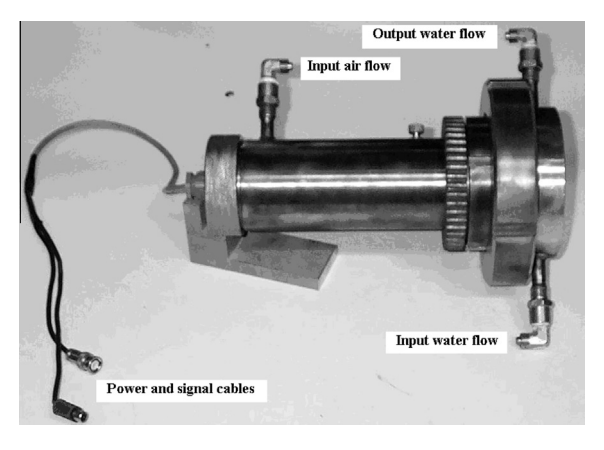


Fig. 3. Housing details.

thermocouple was used for temperature measurement, infra red gas analyzers for measurement of CO, CO_2 and SO_2 contents, a paramagnetic analyzer for O_2 concentration and a chemiluminescent gas analyzer for NO_x content measurement.

Flame images were captured by a standard monochromatic RS-170 CCD camera (Marshall Model 1070) using an objective lens (6 mm, f1.2) supplied with a narrow band-pass (± 10 nm) interferometric filter at the 900 nm reference wave length, near to the sensitivity luminance peak (750 nm) of the CCD sensor and in the range of radiation of the soot, that corresponds to the major part of the radiation emitted by a typical fuel oil flame. All these optical components lie inside an air–water cooled housing (Fig. 3) with a double glass window, which is inserted into the furnace through a proper orifice. The CCD camera output composed-video signals are sampled at 25 Hz by a frame grabber (Sensoray Model 611) as a series of interlaced 640 \times 480 pixels images that are finally transferred to the computer memory through specific frame grabber driver functions.

Using the equipments and instruments referred above, a series of experiments to produce combustion processes with controlled vapor flow rates gave rise to a collection of flame images that were further off-line processed by the image-based diagnostic system whose main tasks are described in the next topics.

3. Image flame analysis

Although combustion process characterization could be made on the basis of a large number of image feature properties, encompassing geometry, luminance and spectral aspects of the flame image, it was established that, to attend real-time performance requirements, only the simplest and fastest algorithms should be applied. Considering that the shape of image grey-level histograms changed for flames with different vapor flow rates (Figs. 4(a) and (b), 5(a) and (b)), ten geometric properties of these histograms have been selected to compose the characteristic vector $\{v_i\}$ of a particular image flame I_i : $v_{i1} = x$ -coordinate of the centroid; v_{i2} = y-coordinate of the centroid; v_{i3} = x-projection of the radius of gyration; v_{i4} = y-projection of the radius of gyration; v_{i5} = coordinate x corresponding to 33% of the accumulated area of the histogram; v_{i6} = coordinate x corresponding to 66% of the accumulated area of the histogram; v_{i7} = coordinate x of the highest peak of the histogram; v_{i8} = coordinate y of the highest peak of the histogram; v_{i9} = coordinate x of the second highest peak of the histogram; v_{i10} = coordinate y of the second highest peak of the histogram.

The characteristic vectors $\{v_i\}$ referred before have been calculated to every instantaneous image I_i of a training set with 214 deinterlaced flame images corresponding to nine different VFR values (0.17,0.21,0.23,0.26,0.29,0.36,0.43,0.50,0.57) associated to nebulization patterns of increasing qualities; at the same time, their respective fuzzy classifications to the fuzzy set 'Flames with high nebulization quality' have been made by an expert in combustion processes (Fig. 6).

After calculating the average histograms and the respective average characteristic vectors $\{\bar{\nu}_i\}(i=1,\ldots,10)$ for each of these nine image subsets, it has been established a straightforward method to determine the membership degree vector $\{x_i\}$ of a training set image I_i to the fuzzy set U = 'Flames with high nebulization quality':

```
Let v_{i,j} be an element of the matrix of 214 characteristic vectors \{v_j\} where j \in \{1,\ldots,10\}. Then for every vector v_i, i=1,\ldots,214, for every component v_{i,j}, j=1,\ldots,10 calculate d_j=\min\{|v_{i,j}-\bar{v}_{k,j}|\}, k=1,\ldots,10 determine k_{\min}|d_j=\min\{|v_{i,j}-\bar{v}_{k,j}|\}, k=1,\ldots,9 determine x_{i,j}=\mu(U,k_{\min})
```

Applying the above fuzzy measurement algorithm, vector $\{x\}$ has been calculated for all the 214 images of the training set. Table 1, shows a collection of such measurements for five images of low nebulization quality, grabbed at VFR = 0.21.

4. Estimation problem

The literature (Balbi, Santoni, & Dupuy, 1999, and Mandel et al., 2008) reports some attempts to model the dynamics of flame propagation through discretization of reaction-diffusion partial differential equations in one or two dimensions by finite differences and to estimate the state, the temperature distribution and the remaining amount of fuel, using the Kalman filter. Mandel et al. (2008), for example, generate synthetic ensembles for the Kalman filter from the numerical solution of the reaction-diffusion equation. Combustion parameters of the model result from monitoring real woodland fire; as a result, the uncertainties are restricted to the PDE discretization. Likewise, in Hong, Uang, and Ray (2000), the truncated solution of the wave equation incorporating effects of acoustic waves and combustion dynamics is the basis for a state-space model that intends to describe the dynamics of flames in a generic gas-turbine engine combustion chamber. Both Mandel et al. (2008) and Hong et al. (2000) admit the difficulty in describing combustion behavior based on theoretical models. This brief discussion is meant to introduce and justify the state-estimation approach for determining the quality of oil flames here adopted.

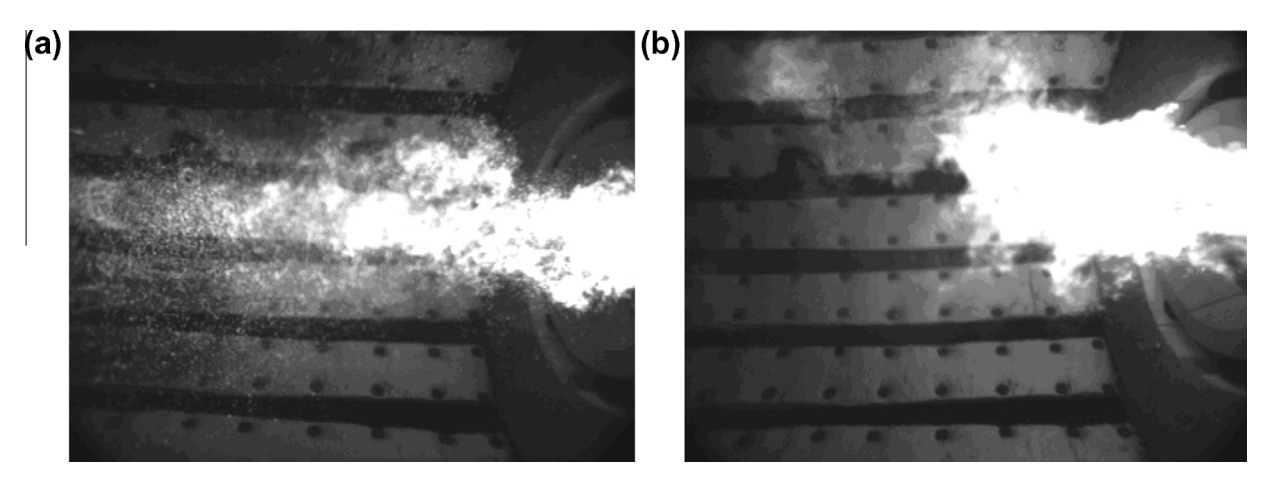
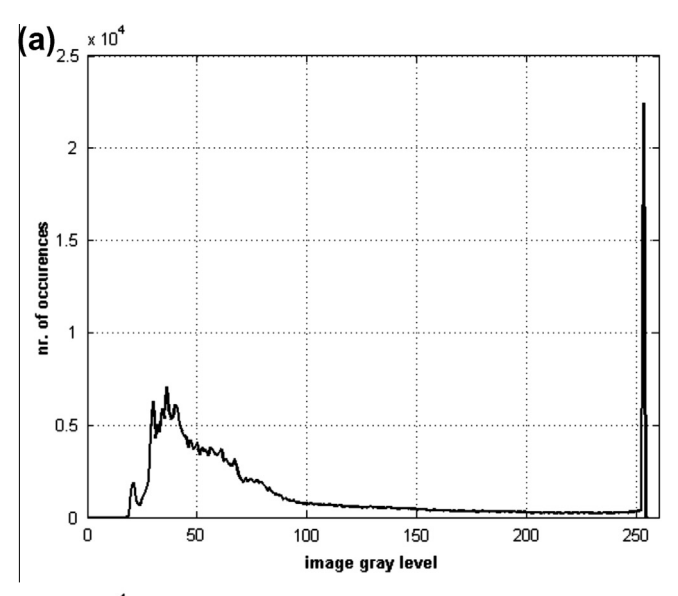


Fig. 4. Image flames with: (a) VFR = 0.17; (b) VFR = 0.57.



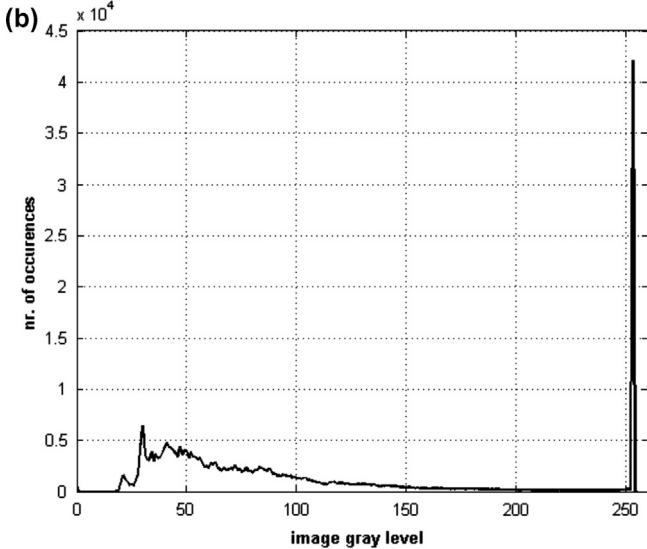


Fig. 5. Histograms of the images of Fig. 5: (a) VFR = 0.17; (b) VFR = 0.57.

In order to tailor the problem to suit the proposed framework, the state to be estimated is defined as a vector containing ten image parameters obtained as described on the previous section. A Kalman filter including a generalized Tikhonov regularization is

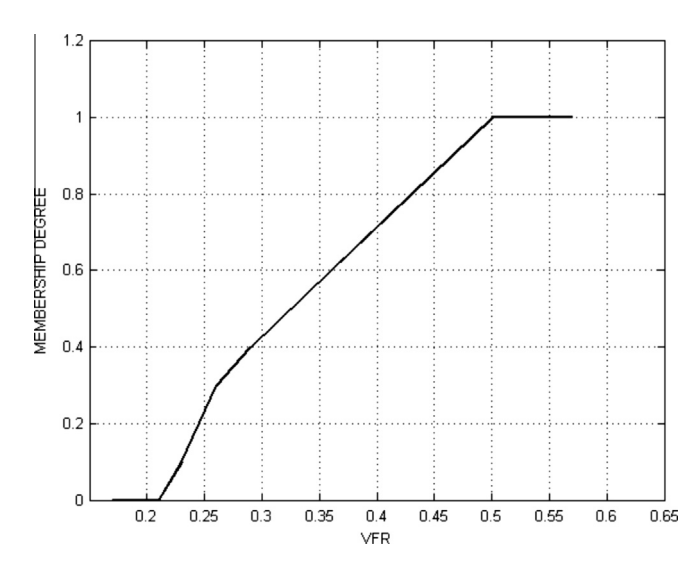


Fig. 6. Fuzzy set associated to the 'High nebulization quality' concept.

implemented to observe the state. The rationale for such inclusion is as follows: during the solution of the inverse problem in a previous work (Fleury et al., 2010), it was observed that, due to the ill-posed nature of the problem, several estimates of the state variables lied beyond the solution space, the closed real interval [0.0; 1.0], thus impairing convergence behavior of the filtering algorithm as a whole. The Tikhonov regularization is a map that converts an ill-posed problem into a well-posed mathematically equivalent one; as a consequence, estimates are expected to be less susceptible to truncation errors.

A thorough discussion on stochastic estimation and on Kalman filtering is out of the current scope; nevertheless, the authors consider necessary to briefly present the basic concepts involved in the derivation of the filter equations, especially when the Tikhonov regularization is to be included. References such as Gelb (1974) and Jazwinski (2007) address the subject in detail.

A necessary condition is that both system and observation models must be in state-space form. The state, in this case, is defined as the ten-parameter vector containing geometrical statistical properties of the grey level histogram of grabbed images. The difficulty in obtaining the system model (a state equation that describes the evolution of the state) arises when one realizes that there is no straightforward physical relationship between the state variables and the grabbed images themselves. A model that can be used

Table 1 Membership degree vector $\{x\}$ to fuzzy set U = `Flames with high nebulization quality'. Calculated for images of low nebulization quality $(\beta = 0.21)$.

Images	{x}									
	<i>x</i> ₁	χ_2	<i>X</i> ₃	<i>X</i> ₄	<i>x</i> ₅	<i>x</i> ₆	<i>x</i> ₇	<i>x</i> ₈	<i>X</i> ₉	<i>x</i> ₁₀
1	0.00	0.00	0.00	0.40	0.00	0.00	1.00	0.00	0.10	0.00
2	0.00	0.00	0.00	0.00	0.00	0.00	1.00	0.00	0.00	0.00
3	0.30	0.30	0.40	1.00	0.30	0.30	1.00	0.40	0.30	0.00
4	0.00	0.00	0.00	0.00	0.00	0.30	1.00	0.00	0.00	0.00
5	0.00	0.00	0.00	0.40	0.00	0.00	1.00	0.00	0.00	0.00

when there is little knowledge on the process is the random walk model, whose state-equation shows that system dynamics is governed by a noise vector, as given by the discrete-time equation, Eq. (1)

$$\underline{\mathbf{x}}(t_k) = \Phi(t_k, t_{k-1})\underline{\mathbf{x}}(t_{k-1}) + \underline{\omega}(t_k), \tag{1}$$

where $\underline{x}(t_k) \in R^n$ is the state at the kth time step $k\Delta t$, $[\Phi(t_k, t_{k-1})]$ is the transition matrix, in this case the identity matrix of order n, and $\underline{\omega}(t_k) \sim N(0, Q(\underline{x}(t_k))) \in R^n$ is a white zero-mean Gaussian noise vector with symmetrical positive semi-definite covariance matrix $Q(\underline{x}(t_k)) \in R^{nxn}$, a necessary condition for Kalman filter implementation.

The observation model is built assuming the hypothesis that each state-vector computed by the fuzzy classification algorithm carries an inherent uncertainty, which can be modeled as a measurement noise that corrupts the state-vector. Mathematically, then, measurements are given by Eq. (2),

$$y(t_k) = H\underline{x}(t_k) + \underline{v}(t_k), \tag{2}$$

where $\underline{y}(t_k) \in R^n$ represents the measurement at t_k , H is an identity matrix of order n, and $\underline{v}(t_k) \sim N(0,R(\underline{y}(t_k))) \in R^n$ is a white zero-mean Gaussian noise vector with symmetrical positive definite covariance matrix $R(\underline{y}(t_k)) \in R^{n \times n}$. The white sequences $\underline{w}(t_k)$ and $\underline{v}(t_k)$ are assumed mutually independent; therefore, they are also uncorrelated, since they are Gaussian.

One of the approaches used to derive the Kalman filter equations consists in minimizing a functional such as

anc

$$H^{\diamondsuit} = \begin{pmatrix} H \\ \alpha I_n \end{pmatrix} \in R^{2n \times n} \tag{7}$$

the functional of Eq. (4) may be written as

$$J(\underline{x}(t_k)) = \frac{1}{2} \left\{ \begin{aligned} & \underline{[\underline{x}(t_k) - \hat{\underline{x}}(t_k)]}^T [P_k^{-1}] \underline{[\underline{x}(t_k) - \hat{\underline{x}}(t_k)]} \\ & + \underline{[\underline{y}^{\diamondsuit}(t_k) - H^{\diamondsuit} \underline{x}(t_k)]}^T \begin{bmatrix} R(\underline{y}(t_k)) & \mathbf{0} \\ \mathbf{0} & I_n \end{bmatrix}^{(-1)} \underline{[\underline{y}^{\diamondsuit}(t_k) - H^{\diamondsuit} \underline{x}(t_k)]} \\ & + \underline{\omega}^T(t_k) [Q^{-1}(\underline{x}(t_k))] \underline{\omega}(t_k) \end{aligned} \right\}$$

$$(8)$$

A functional such as that in Eq. (8), when minimized in relation to $\underline{x}(t_k)$, will provide a regularized Tikhonov solution. Given the similitude between Eqs. (3) and (8), it is possible to conclude that the minimization problem falls into the classical pattern, as stated by Jazwinski (2007). Therefore, the optimal solution will minimize, in a least squares sense, the trace of the error covariance matrix, P_k . The resulting equations constitute a set of forecast-update stages, as follows: For the model given by Eqs. (1) and (2), there is a propagation stage that attempts to provide the best estimates by extrapolating the previous estimated state based on the process model and its known (or admitted) statistics before new information is available. This way, Eq. (9)

$$\hat{\underline{x}}^{(f)}(t_k) = \Phi(t_k, t_{k-1})\hat{\underline{x}}^{(u)}(t_{k-1}) \tag{9}$$

accounts for the state estimation forecast at instant (t_k) (the (f) and (u) superscripts stand respectively for 'before the arrival of new data' and 'after the arrival of new data'), whereas Eq. (10)

$$J(\underline{x}(t_k)) = \frac{1}{2} \left\{ \frac{[\underline{x}(t_k) - \hat{\underline{x}}(t_k)]^T [P_k^{-1}] [\underline{x}(t_k) - \hat{\underline{x}}(t_k)] + [\underline{y}(t_k) - H\underline{x}(t_k)]^T [R^{-1}(\underline{y}(t_k))] [\underline{y}(t_k) - H\underline{x}(t_k)]}{+\underline{\omega}^T(t_k) [Q^{-1}(\underline{x}(t_k))] \underline{\omega}(t_k)} \right\}$$
(3)

in relation to the independent vector (Jazwinski, 2007). When a regularization term like

$$RT = \frac{1}{2} \alpha^2 [\underline{x}(t_k) - \underline{x}^*(t_k)]^T [\underline{x}(t_k) - \underline{x}^*(t_k)]$$

$$\tag{4}$$

is included in the functional of Eq. (3), one obtains an augmented functional

$$P\left(\hat{\underline{x}}^{(f)}(t_{k})\right) = \Phi(t_{k}, t_{k-1})P\left(\hat{\underline{x}}^{(u)}(t_{k-1})\right)\Phi^{T}(t_{k}, t_{k-1}) + Q\left(\hat{\underline{x}}^{(u)}(t_{k-1})\right)$$
(10)

gives the estimation error covariance matrix forecast. An update stage provides proper correction, through the Kalman gain matrix, to the forecasted estimates of the state and error covariance upon the arrival of new measurement data. It must be emphasized that,

$$J(\underline{x}(t_k)) = \frac{1}{2} \left\{ \frac{[\underline{x}(t_k) - \hat{\underline{x}}(t_k)]^T [P_k^{-1}] [\underline{x}(t_k) - \hat{\underline{x}}(t_k)] + [\underline{y}(t_k) - H\underline{x}(t_k)]^T [R^{-1}(\underline{y}(t_k))] [\underline{y}(t_k) - H\underline{x}(t_k)]}{+ \underline{\omega}^T (t_k) [Q^{-1}(\underline{x}(t_k))] \underline{\omega}(t_k) + \frac{1}{2} \underline{\alpha}^2 [\underline{x}(t_k) - \underline{x}^*(t_k)]^T [\underline{x}(t_k) - \underline{x}^*(t_k)]} \right\},$$

$$(5)$$

in which $\alpha > 0$ is a regularization parameter and $\underline{x}^*(t_k)$ is any initial estimate for $\underline{x}(t_k)$. Defining augmented observation matrices

$$\underline{y^{\Diamond}}(t_k) = \left(\frac{\underline{y}(t_k)}{\alpha I_n \underline{x}^*(t_k)}\right) \in R^{2n} \tag{6}$$

due to the Tikhonov regularized formulation, although the augmented state is updated, only the n-dimensional upper partition of the augmented state vector is considered for the next forecast stage.

The Kalman gain matrix is computed according to Eq. (11),

$$K_k^{\diamondsuit} = P(\hat{\mathbf{x}}^{(f)}(t_k)) \left[P(\hat{\mathbf{x}}^{(f)}(t_k)) + R^{\diamondsuit}(t_k) \right]^{(-1)}, \tag{11}$$

where

$$R^{\diamond}(t_k) = \begin{bmatrix} R(\underline{y}(t_k)) & 0\\ 0 & I_n \end{bmatrix}$$
 (12)

The updated state and error covariance matrix are obtained from

$$\underline{\hat{\mathbf{x}}}^{(u)}(t_k) = \underline{\hat{\mathbf{x}}}^{(f)}(t_k) + K_k^{\Diamond} \left(\underline{\mathbf{y}}^{\Diamond}(t_k) - H^{\Diamond} \underline{\hat{\mathbf{x}}}^{(f)}(t_k) \right)$$
(13)

$$P\left(\underline{\hat{x}}^{(u)}(t_k)\right) = \left(I_n - K_k^{\Diamond} H^{\Diamond}\right) P\left(\underline{\hat{x}}^{(-)}(t_k)\right)$$
(14)

thus completing the prediction-correction steps necessary for the next iteration.

5. Nebulization quality estimation

It is common, for simplicity, when there is a lack of knowledge on uncertainty of process and observation models, to admit both noise covariance matrices diagonal. In this work, however, noise covariance matrices shall not be assumed diagonal, once it is possible to compute them from the available data.

The process covariance matrix Qused in Eq. (10) is obtained in the following manner: According to the dynamical model from Eqs. (1) and (2), state and measurement are the same for each training set (data set). It is admitted that the state, on each case, is corrupted by a white zero-mean Gaussian noise sequence that represents the uncertainty generated by the fuzzy measurement algorithm. In order to quantify this uncertainty, the complete history of state vector evolution, which is known for all sets, is assembled in a matrix $\Lambda(\underline{x}(t_k)) \in R^{nxm}$, with n = 10 (the dimension of the state vector) and m = 214 (the complete history of state evolution); afterwards, the covariance of the state considering the complete set of measurements, matrix $\Gamma \in R^{nxn}$, can be calculated through Eq. (15)

$$\Gamma = E\left\{ \left[\Lambda - E(\Lambda) \right] \cdot \left[\Lambda - E(\Lambda) \right]^T \right\}$$
(15)

Matrix Γ states the uncertainties of an actual process whose nebulization quality is unknown *a priori*, since its computation involved data in the range from "high" to "low" nebulization quality characteristic experiments; on that ground, although the actual state covariance for a particular set is not available, matrix Γ can be considered an estimator of matrix Q for each individual process, thus completing the random walk model for the state evolution.

As to the observation model, measurements are synthetically generated for each set by adding to the state a white zero-mean Gaussian noise sequence with standard-deviation that amounts to 10% of the maximum value assumed by the state variables throughout the process. This choice of the state noise level takes into account the uncertainties due to luminance saturation, electronic noise, and quantization errors added when the images are transferred to the computer. The noise sequence is calculated using a routine from Press, Vetterling, Teukolsky, and Flannery (1992), operating within a driver developed by the authors.

The estimation procedure was evaluated by running the Kalman filter algorithm with the model from Eqs. (2) and (3), state covariance matrix Q and measurement noise covariance matrix Q computed by Eq. (15) using vector \underline{y} for each set of measurements, instead of matrix Q, and using three training sets, namely Q and 0.57, respectively reproducing "low", "medium" and "high" quality nebulization patterns. The initial state vector assumes a "high" quality nebulization pattern, i.e., the state variables are given the minimum admitted value, 0.0. Initial error covariance matrix, $Q(\underline{x}(t_0))$ is assumed diagonal with variances 0.3 for all experiments.

Table 2 Summary of previous results.

Vapor flow rate (VFR, %)	Fuel flow rate (kg/h)	Nebulization quality	Mean state, E[<u>x</u> *]
0.17	12	Low	0.17
0.29	20	Medium	0.45
0.57	35	High	0.76

According to what was mentioned in the introduction, the procedure for validating the method consists in applying the Tikhonov regularized Kalman filter to sets whose nebulization pattern quality is considered unknown *a priori* and, upon the results obtained from the filtering process, infer this condition. In a previous work (Fleury et al., 2010), the present authors showed that the mean value of the state variables could be used to evaluate the nebulization condition of measurement training sets by assuring statistical convergence of the estimates from a linear Kalman filter.

Tikhonov regularization is a key feature on the approach here adopted, since it imposes to the state-vector an *ad hoc* convergence for a desired point in the *n*-dimensional solution space while, at the same time, keeps the minimum least-square features of the filtered estimates. Thus, once the unknown nebulization pattern quality of a set is 'forced' by the Tikhonov-regularized solution to an arbitrary point in the solution space, statistical convergence criteria shall be able to assert actual divergence of the estimates; consequently, for each set, one tests convergence of the estimates for 'low', 'medium' and 'high' quality points in the solution space. The rejection of two of the previous conditions must imply in the acceptance of the remaining, as will be shown in the next section of the paper.

6. Results and discussion

Since the benchmark for the validation of the method proposed here is Fleury et al. (2010), it is convenient to recall the main results there presented, as summarized on Table 2 in which the fourth column is the point $E[\underline{x}^*]$ in the solution space to be sought by the Tikhonov-regularized Kalman filter algorithm (forced solution).

Actual convergence of the estimation process was asserted by the inspection of the observation residuals (Fleury, 1985, and Jazwinski, 2007), the difference between the effective measurement and its value as calculated by the filter using the last available state estimate. An estimation process is considered convergent once the normalized observation residuals, given by Eq. (16),

$$r_{v} = \frac{1}{\ell \sigma_{v}} \sum_{i=1}^{\ell} \left(y_{j}(t_{k}) - \hat{x}_{j}^{(f)}(t_{k}) \right), \tag{16}$$

where ℓ represents measurement vector dimension and σ_{ν} is the standard-deviation of measurement noise, are zero-mean Gaussian with standard deviation between $-3\sigma_{\nu}$ and $3\sigma_{\nu}$. The same criterion is used in this work to ensure statistical convergence (or divergence) of the estimates.

The estimation procedure with the proposed approach was conducted using data from four distinct fuel flow rates, namely, 15, 25, 30 and 40 kg/h; the Tikhonov regularization parameter α was assigned the value 1.0 to all conditions. The results obtained with the four conditions above are depicted in Figs. 7–10, which graphically present the evolution of the state variables mean value in each iteration,

$$E\Big[\hat{\underline{x}}^{(f)}(t_k)\Big] = \frac{1}{n} \sum_{i=1}^{n} \hat{x}_j^{(f)}(t_k)$$
 (17)

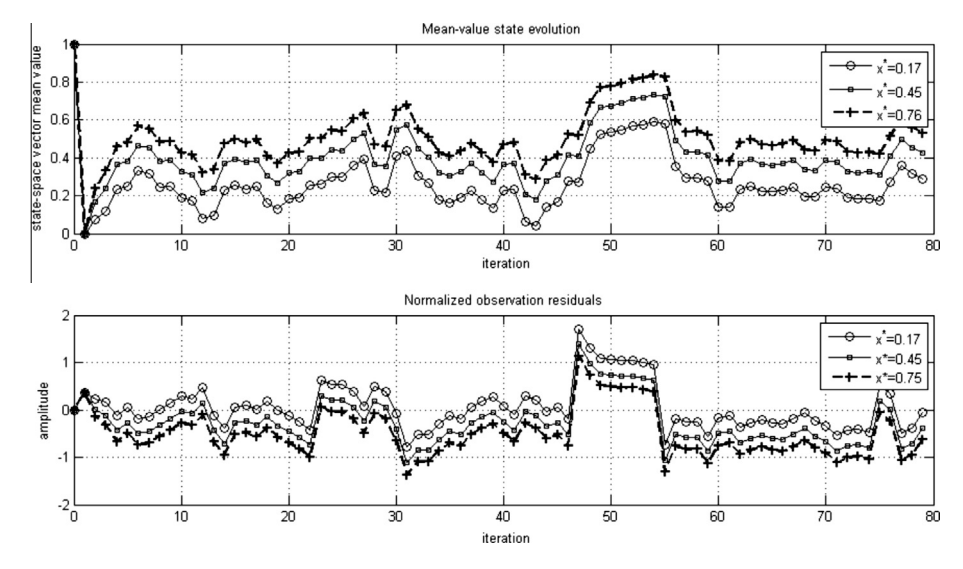


Fig. 7. Quality membership degree estimates for fuel flow rate = 15 kg/h.

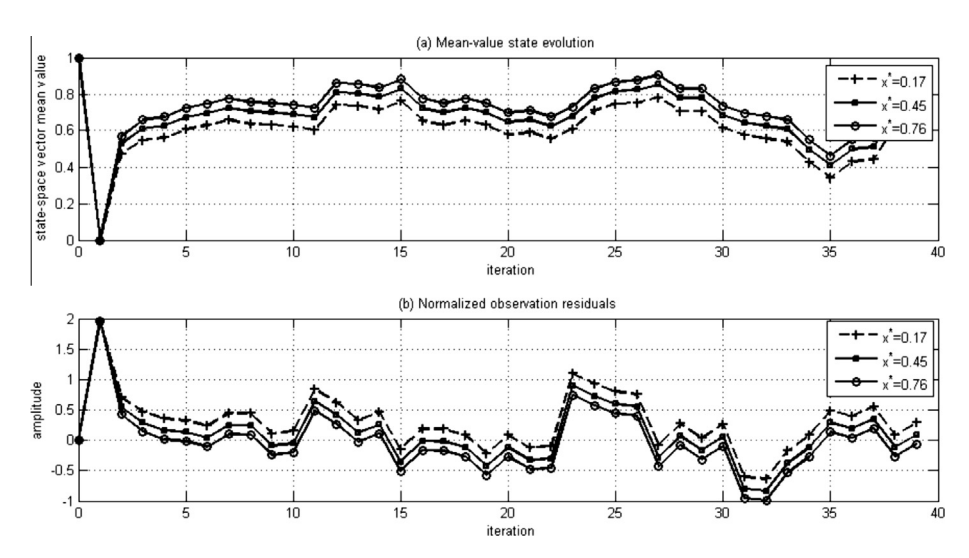


Fig. 8. Quality membership degree estimates for fuel flow rate = 25 kg/h.

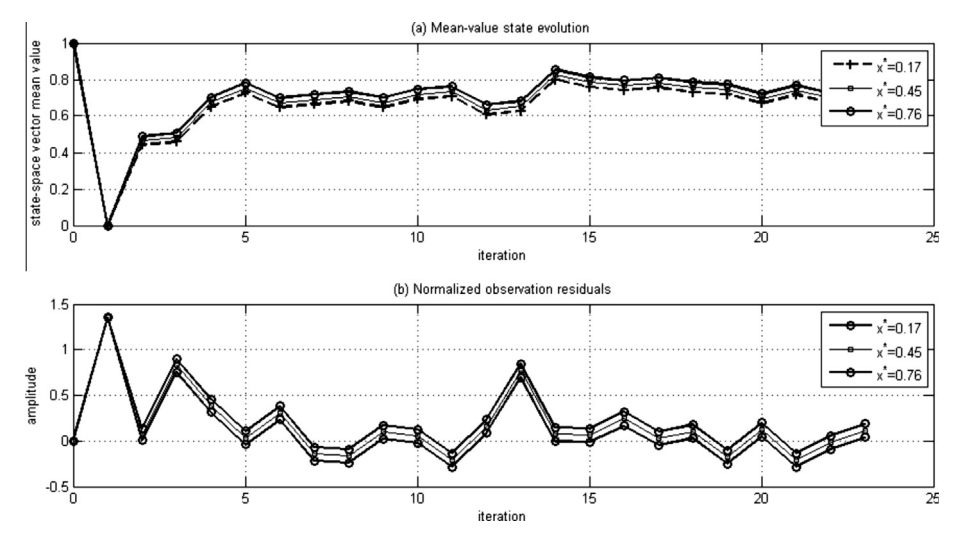


Fig. 9. Quality membership degree estimates for fuel flow rate = 30 kg/h.

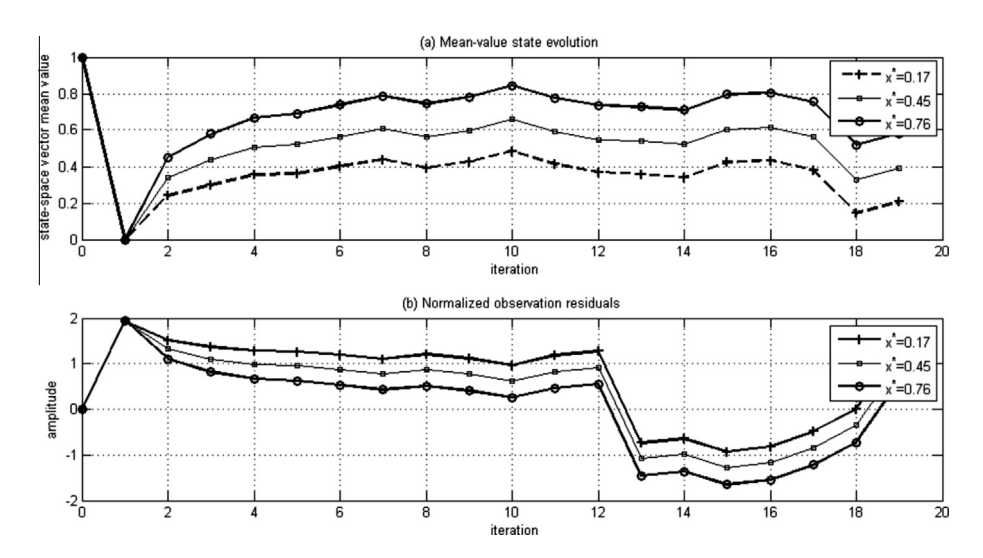


Fig. 10. Quality membership degree estimates for fuel flow rate = 40 kg/h.

Table 3Application of convergence criterion to test data.

Fuel flow rate (kg/h)	$E[\underline{x}^*]$	$E[r_v], \sigma_{r_v}$	Convergence (Y/N)	Estimated nebulization quality
15	0.17	0.059,0.482	Y	Low
	0.45	-0.210, 0.486	N	
	0.76	-0.505, 0.496	N	
25	0.17	0.299, 0.462	N	High
	0.45	0.138, 0.478	N	_
	0.76	-0.038, 0.497	Y	
30	0.17	0.230,0.356	N	High
	0.45	0.164, 0.364	N	
	0.76	0.091,0.375	Y	
40	0.17	0.658, 0.923	N	High
	0.45	0.327, 0.962	N	_
	0.76	0.038, 1.012	Y	

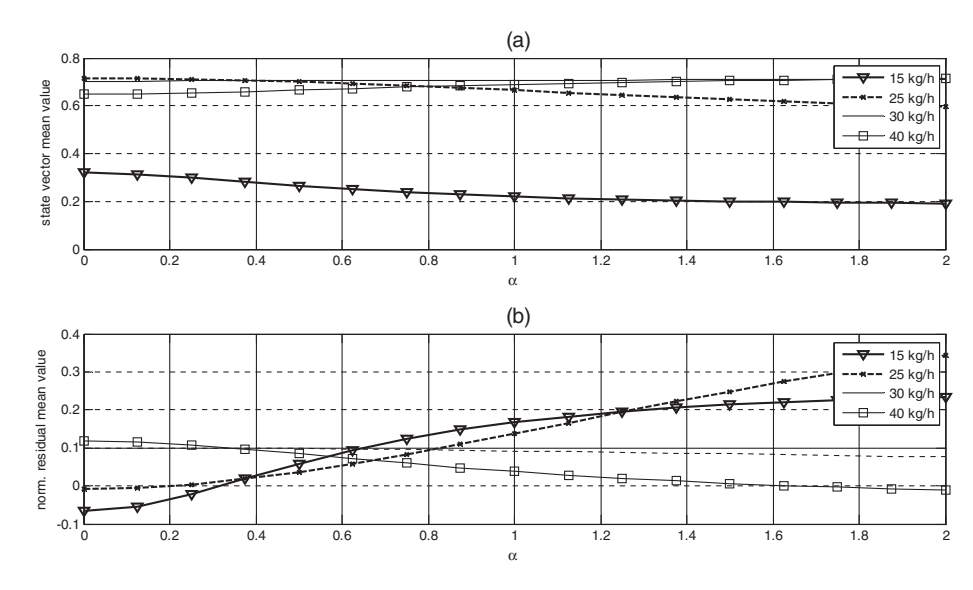


Fig. 11. Sensitivity analysis on the influence of the parameter α : (a) mean value of the state vector; (b) mean value of the normalized residual.

as well as the normalized observation residuals as functions of the time step throughout the process. Results of application of convergence criterion, Eq. (16), are listed on Table 3. The reason for distinct end of scales of the abscissas is the available number of measurements in each case.

From the 'a' subfigures 7 to 10, it is possible to notice that the overall behavior of the estimates, regardless of fuel flow rate, presents a constant shift in the ordinate axis direction among points on the same time step, which can be explained by the 'forcing' action of the Tikhonov regularization parameter to a constant $E[\underline{x}^*]$

Table 4Application of convergence criterion to test data with corrected Tikhonov parameter.

Fuel flow rate (kg/h)	<i>E</i> [<u>x</u> *]	$E[r_v], \sigma_{r_v}$	Convergence using $\alpha = 0.19 (Y/N)$	Estimated nebulization quality
25	0.17 0.45 0.76	1.0e-2, 0.497 1.0e-3, 0.498 -9.1e-3, 0.499	N Y N	Medium

value. Further evidence of the previous assertion is provided by the evolution of normalized observation residuals in the 'b' subfigures 7 to 10. This is consistent with the fact that, since the process model adopted is the random walk with constant process noise covariance matrix for all testing sets, it is to be expected that the updates of the state be more influenced by uncertainties in the measurements (matrix R^{\diamond}) used to compute the Kalman gain, which is conditioned to a constrained regularized least-squares solution of an optimization problem.

Regarding the application of the convergence criterion to the tested sets one realizes, from Table 3, that the leading parameter to ensure effective convergence is the residual mean value, once the twelve tested conditions exhibited similar standard-deviations which, moreover, remained within established limits. It must be emphasized that for the testing data sets corresponding to fuel flow rates of 15, 30 and 40 kg/h, the estimated nebulization quality levels confirmed what was expected when the tests were devised in Fleury et al., 2010. Nevertheless, for the 25 kg/h flow rate, a test designed to fulfil the medium quality requirements, the result obtained suggests a classification error, whose possible causes require further investigation.

Classification errors are typical in processes based on training sets (Theodoridis & Koutrombas, 2009). Attention must be paid to the fact that data randomly selected as a training set is generally composed of a small number of elements, (which is the case in this work), and small samples are more prone to present some bias. Therefore, the selection of the testing set may not match exactly the classification ranges based on the training set. Besides that, from the human specialist point of view, the classification threshold between flames exhibiting patterns of low/medium and medium/high quality is slight, thus becoming another source of uncertainties.

Instead, one might argue whether the source of the classification error arises from under or overweighing the estimates of the state through a poor choice of the Tikhonov parameter, α . Aiming at investigating such a possibility, a sensitivity analysis on the influence of this parameter on the mean estimated state vector and on the mean normalized residual was performed using data from the 15, 25, 30 and 40 kg/h fuel flow rate testing sets, with the forcing condition $E[\underline{x}^*]$ respectively to 0.17, 0.45, 0.76 and 0.75. Graphical results are given in Fig. 11, from which special interest must be drawn to the point (0,0) of the mean normalized residual curve, plot (b), because, as previously stated, the convergence criterion concerning the zero-mean prevailed over the standard-deviation requirement. The optimal computed α , i.e., the one that provides the best stochastic least-squares mean constrained fitting of this testing set to the desired point obtained on each of the training sets, although not clear in the plot, equals correspondingly 0.62, 0.19, ∞ , and 1.66; hence, using $\alpha = 1$. In the mentioned simulation of the low quality nebulization condition overestimates the mean state vector, possibly leading to the obtained misclassification.

In order to corroborate this statement, the estimation process was repeated for the 25 kg/h data, yet this time setting α = 0.19 and testing for the three nebulization quality conditions. Results are presented in Table 4, from which it is worthwhile noticing

the orders of magnitude reduction in the mean normalized residuals, despite the amplitude of the forcing term. This occurrence was expected, by the intrinsic nature of constraint imposed by the regularization parameter. However, one must realize that the mean value of the convergent condition is, still, one order of magnitude lower than the other two.

7. Conclusion

In this work, a method for the determination of nebulization quality for oil flames in industrial processes was improved and validated. The approach consisted in using images grabbed from CCD cameras to build a fuzzy classification set of rules, and in employing the resulting characteristic vector in a state-space model of flame dynamics.

A non-linear Tikhonov regularized Kalman filter was able to provide estimates of the state from data of training sets whose nebulization pattern quality was unknown *a priori*, and to assign them a quality classification. Correctness of the decision making process was corroborated by the adherence of the statistics of the normalized observation residuals to their expected values. Possible sources of discrepancy were analysed and discussed.

Overall, the results suggest that the method might be applied to real-time monitoring the nebulization pattern quality of an oil refinery furnace, since the data acquisition is based on a single CCD camera and the computational processing of those data takes the order of milliseconds on a conventional personal computer. The current research by the authors of this paper intends to further improve the quality of the estimates by attempting to incorporate flame dynamics on the state-space model through an operational analysis framework.

Acknowledgements

The authors wish to thank the Conselho Nacional de Pesquisa e Desenvolvimento Tecnológico – CNPq (Brazilian National Council of Technological Research and Development), who supported this work as part of the projects 484260/2011-1, 'Caracterização do início do processo de instabilização de chamas em fornos de refino', and 471115/2004-5, 'Sistema de monitoramento em tempo real de chamas em forno de refino'. First author acknowledges also CNPq for funding part of the work.

References

Azadeh, A., Ebrahimipour, V., & Bavar, P. (2010). A fuzzy inference system for pump failure diagnosis to improve maintenance process: the case of a petrochemical industry. *Expert Systems with Applications*, *37*, 627–639.

Balbi, J. H., Santoni, P. A., & Dupuy, J. L. (1999). Dynamic modeling of fire spread across a fuel bed. *International Journal of Wildland Fire*, 9(4), 275–284.

Baldini, G., Campadelli, P., & Lanzarotti, R. (2000). Combustion analysis by image processing of premixed flames. In *Proceedings of international conferences on image processing* (Vol. 2, pp. 708–711). Vancouver, Canada.

Bertucco, L., Fichera, A., Nunnari, G., & Pagano, A. (2000). A cellular neural networks approach to flame image analysis for combustion monitoring. In *Proceedings of the sixth IEEE international workshop on cellular neural networks and their applications* (pp. 455–459). Catania, Italy.

Calisto, H., Martins, N., & Afgan, N. (2008). Diagnostic system for boilers and furnaces using CFD and neural networks. Expert Systems with Applications, 35, 1780–1787

Fleury, A. T. (1985). Estimadores de estado de sistemas dinâmicos baseados no conceito de dualidade. Ph.D. thesis, Universidade de São Paulo.

Fleury, A.T. (Coordinator) (2006). Project report on Sistema de monitoramento em tempo real de chamas em fornos de refino. IPT/CNpq, Brazil.

Fleury, A. T., Trigo, F. C., & Martins, F. P. R. (2010). Application of computer vision and Kalman filtering technics to identify oil flames nebulization quality. *ABCM Symposium Series in Mechatronics*, 4, 1–10.

Gelb, A. (Ed.). (1974). Applied optimal estimation. Boston, USA: MIT Press.

González-Cencerrado, A., Peña, B., & Gil, A. (2012). Coal-flame characterization by means of digital image processing in a semi-industrial scale PF swirl burner. Applied Energy, 94, 375–384.

- Heo, G., Changa, S. H., Choib, S. S., Choic, G. H., & Jee, M. H. (2005). Advisory system for the diagnosis of lost electric output in nuclear power plants. *Expert Systems with Applications*, 29, 747–756.
- Hernández, R., & Ballester, J. (2008). Flame imaging as a diagnostic tool for industrial combustion. *Combustion and Flame*, 155, 509–528.
- Hong, B., Uang, V., & Ray, A. (2000). Robust feedback control of combustion instability with modelling uncertainty. Combustion and Flame, 120, 91–106.
- Jazwinski, A. H. (2007). Stochastic processes and filtering theory. New York, USA:

 Dover
- Lu, G., Gilabert, G., & Yan, Y. (2005). Vision based monitoring and characterization of combustion flames. *Journal of Physics: Conference Series*, 15, 194–200.
- Mandel, J., Bennethum, L. S., Beezley, J. D., Coen, J. L., Douglas, C. C., Kim, M., et al. (2008). A wildland fire model with data assimilation. *Mathematics and Computers in Simulation*, 79, 584–606.
- Press, W., Vetterling, W. Y., Teukolsky, S. A., & Flannery, B. P. (1992). Numerical recipes in C the art of scientific computing (2nd ed.). Cambridge, U.K: Cambridge University Press.
- Qian, Y., Li, X., Jiang, Y., & Wen, Y. (2003). An expert system for real-time fault diagnosis of complex chemical processes. Expert Systems with Applications, 24, 425–432.

- Sahu, H. B., Padhee, S., & Mahapatra, S. S. (2011). Prediction of spontaneous heating susceptibility of Indian coals using fuzzy logic and artificial neural network models. Expert Systems with Applications, 38. 2271–2282.
- Santos-Victor, J. A., Costeira, J. P., Tomé, J. A. B., & Sencieiro, J. J. S. (1993). A computer vision system for the characterization and classification of flames in glass furnaces. *IEEE Transactions on Industry Application*, 29(3), 470-478.
- Theodoridis, S., & Koutrombas, K. (2009). Pattern recognition (4th ed.). Elsevier.
- Tuntrakoon, A., & Kuntanapreda, S. (2003). Image based flame control of a premixed gas burner using fuzzy logics. *Lecture Notes in Computer Science*, 2871(2003), 673–677.
- Wójcik, W., & Kotyra, A. (2009). Combustion diagnosis by image processing. *Photonics Letters Poland*, 1(1), 40–42.
- Yan, Y., Lu, G., & Colechin, M. (2002). Monitoring and characterization of pulverized coal flames using digital imaging techniques. Fuel, 81, 647–656.
- Yan, Y., Lu, G., & Colechin, M. (2004). A digital imaging based multi functional flame monitoring system. *IEEE Transaction on Instrumentation and Measurement*, 53(4), 1152–1158.